Relativistic Model Core Potential Study of the Au^+Xe System

Tao Zeng and Mariusz Klobukowski*

Department of Chemistry, University of Alberta, 11227 Saskatchewan Drive, Edmonton, Alberta T6G 2G2, Canada

Received: February 12, 2008

A computational study of the Au^+Xe ionic system has been performed using newly developed coupled-cluster methods and relativistic model core potentials, with extra basis functions optimized to afford superior polarizabilities. Potential energy curves for the dissociation of Au^+Xe were studied at different levels of theory, and molecular properties (bond length and harmonic vibrational frequency) were calculated. Wave functions were analyzed using the natural bond orbital method. The nature of bonding in this system is discussed.

1. Introduction

Because of their respective noble characters, gold and noble gases were considered unable to form any chemical bonds. However, the nobleness of noble gases was first challenged by the discovery of the first Xe compound in 1962,[1] and Au has a very high chemical activity because of its exceptional relativistic effects.[2–4] In 1995, Pyykkö predicted the existence of Au−Ng (noble gas) compounds based on theoretical studies on Au^+Ng (Ng = He−Xe) systems and concluded that, of all of the stable noble gases, Xe would form the strongest bond with Au^+, with a dissociation energy (D_e) of 0.910 eV and a bond length (r_e) of 2.761 Å as calculated using the CCSD(T) method and quasirelativistic pseudopotentials.[5] Since then, Au^+Xe has been an attractive subject for further study among chemists. Indeed, the Au^+Xe ion was detected by mass spectrometer in 1998, and the values of D_e and r_e were refined to 1.31 eV and 2.574 Å, respectively, by calculations with an improved basis set.[6]

As confirmation of this prediction, the first compound containing a Au−Xe bond, $[AuXe_4]^{2+}([Sb_2F_{11}]^-)_2$ was synthesized by Seidel and Seppelt in 2000.[7] More similar compounds were synthesized by the same group, including $[AuXe_2]^{2+}$ $[Sb_2F_{11}]^-[Sb_2F_6]^-$ and $[AuXe_2F]^{2+}[SbF_6]^-[Sb_2F_{11}]^-$.[8] All of these compounds contain a Au^{2+} or Au^{3+} coordination center. Later, they also synthesized the first compound containing a Au^+−Xe bond, $[(F_3As)AuXe]^+[Sb_2F_{11}]^-$,[9] and measured the bond length to be 2.61 Å. These findings encouraged us to probe the nature of the interaction between Au and Xe. Because Au^+ has an empty 6s shell that is strongly contracted by the relativistic effects, it should exhibit very pronounced ability to accept electron(s). On the other hand, Xe has the most diffuse valence shell among the noble gases and should exhibit the strongest electron donation and electron correlation interaction. Thus, Au^+−Xe is expected to be the most strongly bonded in the hierarchy of noble gas−noble metal interactions. Naturally, Au^+−Xe or other species containing a Au(I)−Xe fragment are candidates for theoretical investigations of this special "noble−noble" interaction.

In two early Au^+Ng articles,[5,6] Pyykkö and co-workers suggested that the covalent character in the Au^+Ng interaction increases as the Ng changes from He to Xe and that the charge transfer from Xe to Au^+ is significant. This suggestion indicates that a dative bond (Xe → Au^+) is formed. Pyykkö emphasized the covalency of this interaction in his commentary[10] on Seidel and Seppelt's discovery of $[AuXe_4]^{2+}([Sb_2F_{11}]^-)_2$. The role of covalency was challenged by Read and Buckingham, who explained the interaction in terms of long-range polarization and dispersion and argued that the covalent role of the interaction was negligible.[11] However, their argument was questioned by Bellert and Breckenridge,[12] who pointed out that Read and Buckingham used an unphysical repulsive term in their model potential and that their analysis could not rationalize Pyykkö et al.'s higher-level calculations.[6] Following the discovery of $[AuXe_4]^{2+}([Sb_2F_{11}]^-)_2$, Hu and Huang performed density functional theory (DFT), quadratic configuration interaction, and coupled-cluster calculations on the $[AuXe_4]^{2+}$ species and found that higher-level correlation methods were necessary to obtain accurate results.[13] Berski et al. carried out topological analysis of the electron localization function of the same ion based on their B3LYP optimized structure and electron density.[14] They suggested that the Au−Xe binding is of a "closed-shell" nature and is dominated by electrostatic interactions. Cooke and Gerry, using microwave rotational spectroscopy, detected and characterized XeAuF, the simplest compound containing Au(I)−Xe, and performed second-order Møller−Plesset perturbation (MP2)[17–21] calculations on the species.[22] They found a very short (2.54 Å) and rigid Au−Xe bond with a bond energy of about 1.04 eV, and their molecular orbital contours indicated significant sharing between Xe and Au. Ghanty carried out theoretical studies on AuXeF and AuXeOH and tried to determine the bonding nature of Au−Xe in those species.[23] His findings point to a covalent, or at least partially covalent, Au−Xe bond. More recently, the nuclear quadrupole moment of gold in XeAuF was studied with the four-component relativistic coupled-cluster[15] and density functional methods.[16]

Is the Au(I)−Xe bond covalent or not? That is the question the researchers cited above tried to answer. However, because of the obscure and subjective definition of covalency and the complexity of the bond, there is no clear answer yet. The objective of this work was to use our newly developed relativistic model core potentials (MCPs), in combination with newly developed coupled-cluster (CC) methods, to obtain a clearer understanding of this interaction, with the aim that our high-level CC calculations can provide references for related experimental or theoretical studies in the future. Natural bond

* To whom correspondence should be addressed. E-mail: Mariusz.Klobukowski@ualberta.ca.

10.1021/jp8012656 CCC: $40.75
Published on Web 05/21/2008

TABLE 1: Dissociation Energies (D_e), Equilibrium Internuclear Distances (r_e), Vibrational Frequencies (ω_e) and Anharmonicity Constants ($\omega_e x_e$)

method	D_e (eV)	r_e (Å)	ω_e (cm^{-1})	$\omega_e x_e$ (cm^{-1})
RHF	0.48	2.848	217.51	10.273
MP2	1.24	2.578	154.74	0.610
MP2 (Xe[4d])[a]	1.21	2.595	152.87	0.611
MP2(Au[5p])[b]	1.13	2.612	146.22	0.595
CCSD	0.99	2.659	135.74	0.569
CCSD[T]	1.10	2.638	142.21	0.556
CCSD(T)	1.09	2.641	141.22	0.553
R-CCSD[T]	1.00	2.644	140.37	0.560
R-CCSD(T)	0.99	2.646	139.51	0.558
CR-CCSD[T]	0.99	2.646	139.59	0.560
CR-CCSD(T)	0.99	2.648	138.89	0.559
CCSD(2)_T	1.07	2.644	140.30	0.558
CR-CCSD(T)_L	1.08	2.636	142.89	0.642
CCSD(TQ)_B	1.08	2.643	140.63	0.552
R1-CCSD(TQ)_A	0.97	2.648	138.83	0.558
R1-CCSD(TQ)_B	0.97	2.648	138.91	0.558
R2-CCSD(TQ)_A	0.97	2.647	139.26	0.559
R2-CCSD(TQ)_B	0.97	2.647	139.17	0.559
CR-CCSD(TQ)_A	0.97	2.646	139.37	0.560
CR-CCSD(TQ)_B	0.98	2.647	139.30	0.560
BP86	1.63	2.515	173.81	0.585
BLYP	1.71	2.502	188.24	0.754
B3LYP	1.49	2.585	140.53	0.545
CCSD(T)[6]	1.31	2.57	149	
B3LYP[6]	0.96	2.84	116	
MP2[22]	1.05	2.56	165	
experiment[9]		2.61[c]	138.3[d]	

[a] Frozen Xe 4d electrons. [b] Frozen Au 5p electrons. [c] Crystal structure analysis for $[(F_3As)AuXe]^+[Sb_2F_{11}]^-$. [d] Raman spectrum for $[(F_3As)AuXe]^+[Sb_2F_{11}]^-$.

orbital (NBO) analyses were also performed to obtain further information about the nature of the bonding in Au^+—Xe.

2. Methodology

We used our newly developed MCPs[24,25] to represent pronounced relativistic effects in Au and Xe. The MCPs were parametrized against all-electron scalar-relativistic calculations at the RESC[26] level. The MCPs could be also generated using DK2 or DK3[29–32] all-electron orbitals and orbital energies as references. Although we expect that the quality of the MCP results should not depend strongly on the scalar-relativistic model chosen to generate the reference quantities, work on DK3-based MCPs is currently in progress. Well-tempered basis sets[27,28] were used for the all-electron relativistic calculations and the parametrization of the MCPs. The MCPs reproduce not only the energies, but also the correct nodal structure of the valence orbitals. Because all-electron scalar-relativistic calculations, both RESC and DK3, indicated that the order of orbital energies for the Au atom is [core]5s4f5p5d6s, there is no reason to include the 5s subshell in the valence space while excluding 4f, as is the case for many studies cited above. Furthermore, according to the all-electron relativistic CCSD calculation of Schwerdtfeger et al.,[33] including a correlation between 5s and 4f electrons would not improve the polarizability of Au^+. Thus, in the present work, we explicitly treated 17 electrons for Au ($5p^65d^{10}6s^1$) and 18 electrons for Xe ($4d^{10}5s^25p^6$). Because the scalar-relativistic effect takes place mainly when an electron gets to the vicinity of a nucleus, we expect our MCPs with correct nodal structures to yield better results than general relativistic effective core potentials.

High-level correlation methods are the key to obtaining high-quality results for the Au^+—Xe interaction. In this work, in addition to the conventional CCSD, CCSD[T], and CCSD(T) approaches, we employed a variety of newly developed coupled-cluster methods to calculate the potential energy curve for the dissociation of Au^+—Xe, namely, the renormalized (R-), or completely renormalized (CR-), approaches containing triple (T) or both triple and quadruple (TQ) excitations in the perturbative treatment. They are R-CCSD[T], R-CCSD(T), CR-CCSD[T], CR-CCSD(T), CCSD(2)_T, CR-CCSD(T)_L, CCSD(TQ)_B, R1-CCSD(TQ)_A, R1-CCSD(TQ)_B, R2-CCSD(TQ)_A, R2-CCSD(TQ)_B, CR-CCSD(TQ)_A, and CR-CCSD(TQ)_B. Of these, CR-CCSD(TQ)_B is regarded as the most accurate method. The details of these CC methods are discussed in the articles by Piecuch et al.[34–38] For comparisons and further analyses, restricted Hartree—Fock (RHF), MP2, and DFT calculations were carried out as well. In the MP2 and coupled-cluster calculations, all explicit electrons were correlated, except for two MP2 cases, which were performed to investigate the influence of the penultimate valence shells. For DFT, because we scanned the whole potential curve for the dissociation process, functionals without parametrization were preferable, and we chose BP86 and BLYP[39,40] in the present work. B3LYP[42–46] was chosen to allow for a comparison with previous studies using the same functional. The long-range correction (LC)[47] was turned on to replace the P86 and LYP exchange functionals by the RHF exchange at large interelectron distances. The LC cannot be applied to B3LYP because it has a fixed admixture of RHF exchange.

Our basis sets are based on the original well-tempered basis sets used for MCP preparation. In addition, we least-squares fitted the outermost lobe of the Xe 4d orbital with three f functions (α = 10.86, 3.57, and 1.21); two d functions (α = 4.02 and 1.24) were fitted to the outermost lobe of the Au 5p orbital. These five functions were included in the basis set as the correlating functions for the inner orbitals. Furthermore, the diffuse d (α = 0.05663) and f (α = 0.1595) functions were included to improve the calculated polarizability of Xe. Because Pyykkö et al.[6] emphasized the importance of including g-type functions for this system, we included one such function for each atom, with α = 1.007 for Xe and α = 0.856 for Au. The basis set contraction schemes are (28s23p20d2f1g)/[5s3p7d2f1g] for Au and (28s23p21d6f1g)/[6s5p5d6f1g] for Xe. The Cartesian Gaussian type functions were transformed to spherical harmonic functions. With this basis set, we calculated the polarizability of Xe to be 26.34 au at the MP2 level, which is very close the experimental values of 27.16[48] and 27.815[49] au. The basis set used thus allows for the description of the correlation effects due to the diffuse Xe valence shell.

Given that our primary comparison is with the results obtained by Pyykkö et al.,[5,6] it is worthwhile to contrast the two formalisms used in these calculations. In this work, we used MCPs that were derived from atomic RESC calculations[24,25] that employed well-tempered basis sets.[27,28] The contraction pattern for the basis sets is listed in the preceding paragraph. We employed an 18-electron MCP for Xe ($4d^{10}5s^25p^6$) and a 17-electron MCP for Au ($5p^65d^{10}6s^1$). The pseudopotentials used by Pyykkö et al.[5,6,50,51] were derived from atomic Wood—Boring results[52] and included an averaged spin—orbit potential. The basis set contraction patterns for the highest-level calculation of Pyykkö et al. (basis D in ref 6) were (8s6p5d5f1g)/[7s3p4d5f1g] for Au and (8s8p6d6f)/[7s7p6d6f] for Xe. Pyykkö et al. used an 8-electron pseudopotential for Xe ($5s^25p^6$) and a 19-electron potential for Au ($5s^25p^65d^{10}6s^1$).

We used the methods and basis sets described above to perform single-point calculations for 20 internuclear distances

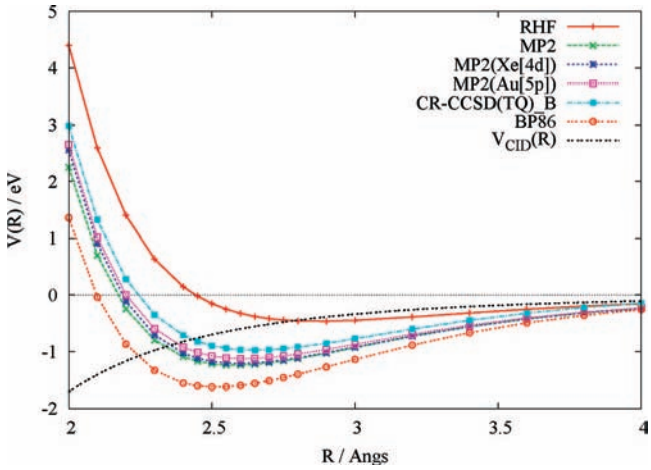

Figure 1. Potential energy curves calculated by the RHF, MP2, CR-CCSD(TQ)_B, and BP86 methods and charge−induced dipole interaction, $V_{CID}(R) = -\alpha_{Xe} q_{Au^+}{}^2/2R^4$.

ranging from 2.00 to 4.00 Å. The bond length (r), interaction energy [$V(r)$], and spectroscopic constants were obtained by fitting an 11-term polynomial to 11 selected sets of [r, $V(r)$] data around the minimum of the potential curve. Of the 20 points, we chose one around the calculated bond length to perform the NBO analysis[53,54] for calculations to obtain the electron density: RHF, MP2, and DFT-BP86. All single-point calculations were carried out with GAMESS-US,[56] and the potential curve fittings were done using an in-house program. The NBO analyses were carried out using the NBO 5.0[55] module attached to GAMESS-US. All contour diagrams were prepared using MacMolplt 7.1.[57]

3. Results and Discussions

3.1. Potential Energy Curves. The spectroscopic constants obtained by fitting the potential curves are reported in Table 1. The dissociation energy refers to the dissociation limit of Au^+ and Xe because the ionization potential of Au is lower than that of Xe. Because of the large number of methods employed, in Figure 1, we illustrate the dissociation potential curves from only four representative methods, namely, RHF, MP2, coupled-cluster, and DFT-BP86; two 'frozen penultimate valence subshell' MP2 curves are included as well to judge the influence of these subshells on the interaction. The charge−induced dipole interaction potential curve is also included as a comparison; it was obtained using the equation[11]

$$V_{CID}(R) = -\alpha_{Xe} q_{Au^+}{}^2/2R^4$$

with the MP2 polarizability $\alpha_{Xe} = 26.34$ au. The interaction energy, $E_{int}(r)$, for each internuclear distance r was obtained by the equation

$$E_{int}(r) = E_{Au^+Xe}(r) - E_{Au^+g(Xe)}(r) - E_{g(Au)Xe}(r)$$

where g represents "ghost" (i.e., the basis set superposition error (BSSE) was taken into account using the counterpoise correction method of Boys and Bernardi).[58] Several other theoretical or experimental data from other studies are included in Table 1 for comparison. The Au^+Xe ion belongs to class B in Pyykkö's classification.[41] Thus, the effect of spin−orbit coupling on the interaction between two closed-shell systems, Au^+ and Xe, should be very small, as only the second-order terms remain, and this effect was not considered in the present study.

In the two special MP2 calculations labeled MP2(Au[5p]) and MP2(Xe[4d]), we excluded excitations from the Au 5p and Xe 4d subshells. From the three MP2 curves and the data in Figure 1 and Table 1, one can clearly see that the Au 5p electrons are more important than the Xe 4d electrons, as freezing Au 5p reduced D_e by 0.11 eV compared to the "all-electron" MP2 value whereas freezing Xe 4d reduced D_e by only 0.03 eV. Obviously, Au 5p must be included in the correlation space but Xe 4d is not essential. Thus, the omission of Xe 4d would significantly reduce the computational effort in coupled-cluster calculations. However, in this work, we correlated all explicit electrons in the coupled-cluster calculations. The difference in importance of the Au 5p and Xe 4d subshells is due to their different radial overlaps with the outer valence orbitals. As shown in Figure 2, the radial distribution function of Au 5p is essentially in phase with that of Au 5d, whereas that of Xe 4d is out of phase with both outer subshells. Therefore, compared to Xe 4d, Au 5p would have greater overlap with the valence shells and exhibit a more pronounced effect on bonding.

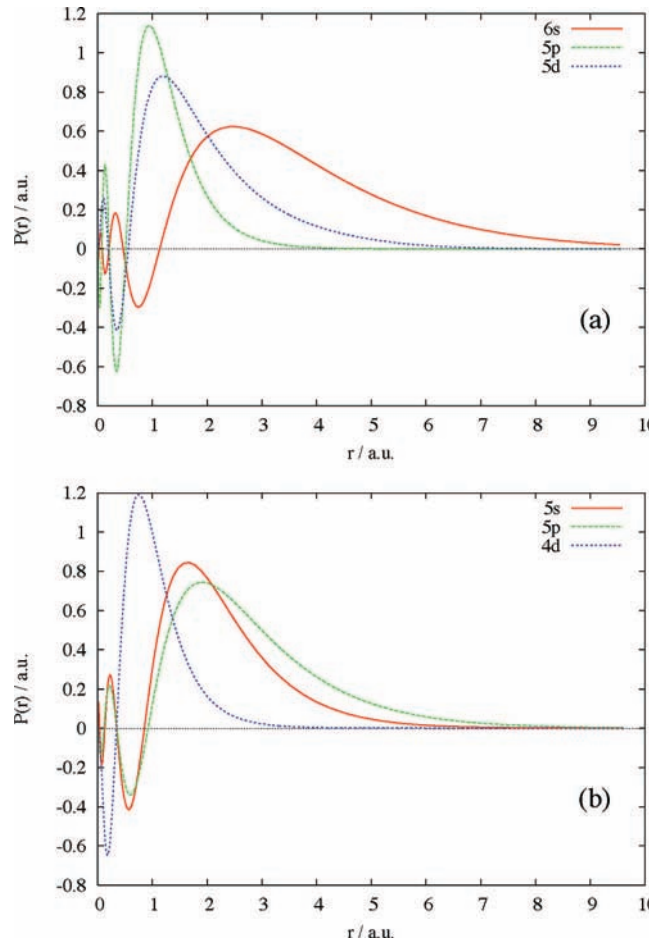

Figure 2. Radial distribution functions, $P(r) = rR(r)$, for atomic (or ionic) orbitals: (a) Au^+ (where 6s is a virtual orbital) and (b) Xe.

From Table 1, one can see that all of the coupled-cluster results are highly consistent, with D_e ranging from 0.97 to 1.10 eV and r_e ranging from 2.64 to 2.66 Å. The R-CC and CR-CC methods did not improve the results dramatically. This can be explained by the small T1 diagnostic index.[59] The R-CC and CR-CC methods are approaches designed for cases including quasidegenerate reference configurations, which cannot be treated by single-reference CC methods. Bond breaking usually requires multiconfigurational wave functions, so single-reference CC methods are not recommended. The T1 diagnostic index is an effective tool for judging whether a system is single-reference

in nature or not. For T1 < 0.02, single-reference is assumed to be safe. In this work, the largest T1 diagnostic index was 0.0134 for r = 2.00 Å. Thus, single-reference CC is satisfactory for this Au^+—Xe dissociation process, and only dynamic correlation must be treated. This special bond breaking is related to the nature of the bonding between Au and Xe, as discussed below. Because CR-CCSD(TQ)_B is the highest level CC approach used in this work, we take its results as the most accurate and the standard for further comparisons, and we refer to this method simply as "the CC" in the remainder of this work.

The CC gave values of 0.97 eV for D_e, 2.647 Å for r_e, and 139.30 cm^{-1} for ω_e. This interaction is weaker than the best CCSD(T) results of Pyykkö et al.,[6] which gave 1.31 eV for D_e, 2.574 Å for r_e, and 149 cm^{-1} for ω_e. Qualitatively, these two results are consistent, considering the different pseudopotentials, basis sets, and levels of coupled-cluster theory in use. More excitingly, the CC closely reproduced the experimental data from crystal structure analysis and Raman spectrum for $[(F_3As)AuXe]^+[Sb_2F_{11}]^-$ of r_e = 2.61 Å and ω_e = 138.3 cm^{-1}.[9] Because Au^+—Xe is only weakly coordinated to F_3As and $[Sb_2F_{11}]_2^-$, we expect this bond length and frequency to be valid for the isolated Au^+Xe fragment. This consistency between the CC and experimental results (2.647 vs 2.61 Å and 139.30 vs 138.3 cm^{-1}) confirms the accuracy of the CC and raises our confidence in the MCPs and basis sets.

Compared to the CC, RHF recovered only one-half of the interaction energy (0.48 eV) and overestimated the bond length (2.848 Å). These results agree with the findings in Pyykkö's first study.[5] Failure to account for electron correlation leads to a steep curve for $r < r_e$, which gives an unreliable vibrational frequency and an unreasonable anharmonicity constant. On the other hand, MP2 overshoots the interaction energy by 0.27 eV (1.24 eV) and underestimates the bond length (2.578 Å). The stronger MP2 interaction was unexpected because Pyykkö found smaller D_e and longer r_e for MP2 than for CCSD(T).[5] Again, this can be ascribed to the different pseudopotentials and basis sets. Despite the numerical differences, the potential curves of the CC and MP2 are closely parallel, and we consider the MP2 results to be acceptable. None of our DFT calculations (BP86, BLYP, and B3LYP) provided satisfactory results compared to the CC. The BP86 potential curve, as the representative of DFT, is far from the CC curve. BP86 and BLYP overestimate D_e by almost a factor of 2 and give a bond that is even shorter than the covalent limit, 2.515 and 2.507 vs 2.57 Å.[22,60,61] Although B3LYP yielded better results than BP86 and BLYP, it still overestimated the interaction. Pyykkö's B3LYP gave a reasonable value of D_e = 0.96 eV but an increased bond length of r_e = 2.84 Å. In their study of $[AuXe_4]^{2+}$, Hu and Huang[13] pointed out that B3LYP could be used to predict interaction energy but not geometry. Their best B3LYP calculation with LANL2 effective core potentials (ECPs) and uncontracted LANL2DZ basis sets for Au—Xe yielded r_e = 2.842 Å, longer than the experimental results (2.728−2.750 Å).[7] Berski et al.[14] used B3LYP with ECP60MDF for Au and ECP46MWB for Xe and the corresponding basis sets to study the same system and obtained a similar elongated r_e (2.878 Å). Judging from these findings, we conclude that B3LYP is not a reliable tool to investigate the Au—Xe interaction. An interesting observation is that B3LYP/ECP tended to predict greater r_e values whereas our B3LYP/MCP approach predicted a shorter bond distance. Because B3LYP and all pseudopotentials were parametrized independently, the poor behavior of B3LYP is understandable. In the future, one should employ coupled-cluster methods for this system, while using MP2 as a substitute when an analysis of electron density is required.

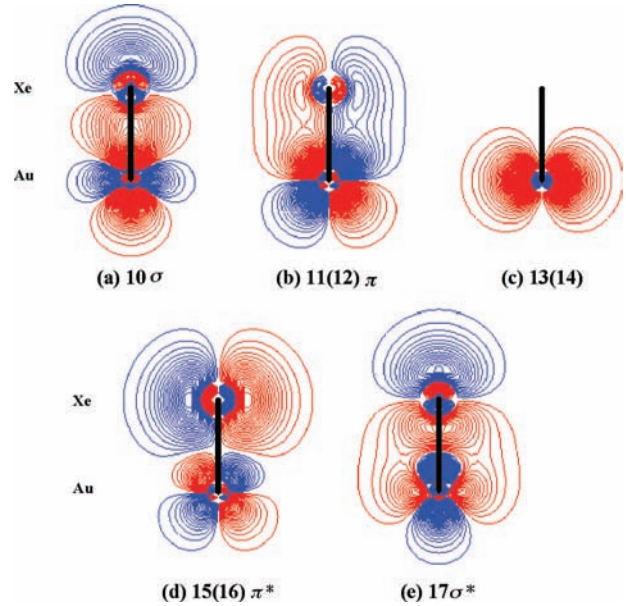

Figure 3. Contour diagrams of occupied frontier molecular orbitals of Au^+Xe, with a maximum contour value of 1.0 au and a maximum number of contours of 100. Red (blue) indicates that the sign of the wave function is positive (negative). All orbital contours in the present work used the same setting of contours unless specified otherwise.

The charge−induced dipole interaction, $V_{CID}(R)$, was used to analyze interactions between closed-shell systems by Read and Buckingham[11] and by Wesendrup and Schwerdtfeger.[62] The $V_{CID}(R)$ potential curve is included in Figure 1 for comparison with other potential energy curves; it was calculated using the equation[11]

$$V_{CID}(R) = -\alpha_{Xe} q_{Au^+}{}^2/2R^4$$

with the MP2 polarizability α_{Xe} = 26.34 au. It is evident that all of the potential curves converge to that for $V_{CID}(R)$ at R = 4 Å. This indicates that, for R > 4 Å, the charge (Au^+)−induced dipole (Xe) interaction prevails.

3.2. Molecular Orbitals. We analyzed the molecular orbitals of Au^+Xe in order to reveal the origin of the weak RHF interaction. The contour diagrams of the frontier MOs up to the highest occupied molecular orbital (HOMO) are shown in Figure 3. These diagrams were obtained from RHF calculations at r = 2.600 Å and provide the same qualitative information as the diagrams for r_e = 2.800 Å, which is closer to the RHF value for r_e.

Parts a and b of Figure 3 represent the 10σ and the degenerate 11(12)π bonding orbitals, respectively, whereas part c represents the degenerate 13(14) Au 5p nonbonding orbitals. The first two contour diagrams imply a triple-bond interaction incommensurate with the weak bonding found at the RHF level, with D_e = 0.48 eV. However, Figure 3d shows the antibonding 15(16)π* orbitals, which cancel the bonding effect from the 11(12)π orbitals in Figure 3b. Figure 3e seems to represent another bonding orbital because there is significant π-type overlap between the nonaxial part of the Xe $5p_z$ orbital and the $x^2 + y^2$ component of the Au $5d_{z^2-x^2-y^2}$ and 6s orbitals. However, it is indeed a σ*-type orbital, as there is a node on the axis between the Xe $5p_z$ orbital and the z^2 component of the Au $5d_{z^2-x^2-y^2}$ orbital. Therefore, Figure 3e indicates that orbital 17σ* is an antibonding partner to orbital 10σ (Figure 3a). Despite its

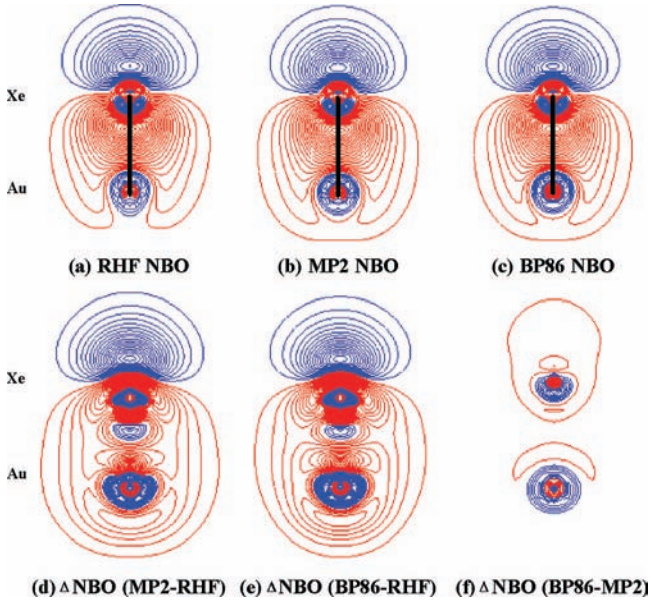

Figure 4. Contour diagrams of natural bond orbitals from RHF, MP2, and BP86 NBO analyses and the differences (Δ) between them. The Δ diagrams (d−f) were plotted with the same maximum contour value, but with 500 as the maximum number of contours to amplify the differences.

antibonding character, $17\sigma^*$ cannot completely cancel out the bonding effect of 10σ, because of the emergence of π-type overlap: The diffuse Xe $5p_z$ orbital already reaches the Au center, so the overlap between Xe $5p_z$ and the toroidal part of Au $5d_{2z^2-x^2-y^2}$ is unavoidable and will contribute to bonding, partially compensating for the antibonding effect of the $17\sigma^*$ orbital. This incomplete σ^* orbital accounts for the RHF D_e value of 0.48 eV. In their study of XeAuF,[22] Cooke and Gerry presented diagrams (Figure 4) for the similar σ and π bonding orbitals, but not the antibonding ones. We expect that orbitals of the same types as $15(16)\pi^*$ and $17\sigma^*$ could be found in the XeAuF study, according to the pairwise nature of molecular orbitals.

3.3. Natural Bond Orbital (NBO) Analysis. For the NBO analysis, $r = 2.600$ Å was chosen as the internuclear distance, and analyses were performed for the RHF, MP2, and BP86 methods. Because coupled-cluster methods do not provide electron densities, we omit the CC from this section (and from section 3.4). Of the three methods included, MP2 should be regarded as providing the best electron density. Natural population analysis (NPA) and NBO results are listed in Table 2, and NBO contour diagrams are presented in Figure 4.

Table 2 indicates that the NBO analyses for the three methods considered are highly credible for the almost-100% Lewis structure percentages. There is only one bonding orbital in each of the NBO analyses, and the high occupancy (1.96 electrons) of the bonding orbital indicates that most of the MP2 interaction can be attributed to the bonding effect. The natural charge of Xe from the NPA indicates a substantial amount of electron transfer from Xe to Au^+ for all three cases, and the amount of electron transfer increases with increasing D_e. The composition of the bonding orbitals suggests that the bonding results from the overlap between the Au 6s and Xe 5p orbitals. In agreement with Pyykkö's results,[5] we did not observe significant participation by the Au 6p orbital. Pyykkö found that the MP2 Mulliken populations were $6s^{0.29}6p^{0.09}$ (Table 4 of ref 5). In this work, we obtained rather similar results, $6s^{0.32}6p^{0.06}$, at the same level of theory. The lack of 6p participation is reasonable because the 6s orbital is more strongly contracted and stabilized than the 6p orbital in Au and the NPA ($6s^{0.29}6p^{0.02}$) indicates that the 6s orbital is far from being saturated.

This Xe 5p → Au 6s electron donation is an indication of a dative bond. The dative nature of the bonding is the reason for the lack of quasidegenerate states during the bond-breaking process, because the bonding electrons all go back to Xe, which has a closed-shell wave function. The small T1 diagnostic index of the coupled-cluster calculations is justified. Correlation effects play an important role in this donation. As illustrated by Figure 4b and d, the MP2 calculations pushed more electron density to the Au side. As can be inferred from the density of the contours, because of the relativistic contraction, the donated electron density resides mainly in the vicinity of the Au nucleus, rather than accumulating in the conventional bonding area. Such an electron distribution requires a correct description not only for the outer lobe of the valence orbital, but more importantly for the inner lobe. This effect could be observed because of the ability of our relativistic MCPs to reproduce the relativistically correct nodal structure for valence orbitals using projection operators. According to Figure 4c, e, and f, BP86 is seen to push too much electron density into the Au center area, as indicated by a greater Au 6s contribution in Table 2. This might be a reason for the overestimation of the bonding strength by the BP86 method.

Each NBO (σ_{AB}) can be written in terms of two directed valence hybrids (NHOs), h and h_B, on the bonded centers A and B, respectively; that is, $\sigma_{AB} = c_A h_A + c_B h_B$.[55] The coefficients c_A and c_B vary smoothly from the covalent ($c_A = c_B$) to the ionic ($c_A \gg c_B$) limit. For the MP2 bond orbital (Table 2), if the contributions from Xe and Au are approximated to be pure 5p and pure 6s, respectively, then the MP2 bonding orbital can be expressed as

$$\sigma_{AuXe} = 0.94(5p_{Xe}) + 0.34(6s_{Au})$$

The coefficients show that this Au^+—Xe bond is a polar bond, rather than an ionic bond. Considering that MP2 overestimated the bonding effect compared to the CC and that the bonding strength is proportional to the electron donation, one would expect that the extent of donation of electron density would be smaller and the bond would be more polar at the Xe end of the ion than observed from the MP2 results. Consequently, based on the NBO analysis, we can conclude that the Au^+—Xe bond is a polar dative bond, closer to the covalent than the ionic limit.

3.4. Density. The electron density for this bonding process was studies as well. Figure 5 shows the changes in electron density (ΔDensity) in the bonding process as determined using the RHF, MP2, and BP86 methods. Again, the calculations were performed for $r = 2.600$ Å. Panels a−c of Figure 5 demonstrate that, as the method changes from RHF to MP2 and to BP86, the electron donation from Xe to Au^+ increases, and the donated electron goes mainly to the vicinity of the Au nucleus and from the vicinity of the Xe nucleus. This is consistent with the NBO analysis. Compared to RHF and MP2, BP86 accumulates more electron density in the bonding area, which could be another reason for its overestimation of the bond strength.

Ghanty, in his study on AuXeF and AuXeOH,[23] found that $\nabla^2\rho$ is positive at the bond critical point (BCP) for the Au—Xe bond. A positive value of $\nabla^2\rho$ at the BCP indicates a closed-shell type interaction, that is, an ionic bond. However, Ghanty's other evidence pointed to a covalent Au—Xe bond. A similar positive value of $\nabla^2\rho$ was also observed by Berski et al.[14] How can one reconcile the covalent nature of the bond and the positive value of $\nabla^2\rho$ at the BCP for this system? Because of

TABLE 2: Results of Natural Population and Natural Bond Orbital Analyses

method	NPA[a] of Xe (*e*)	Lewis structure (%)	occupancy of BD[b] (*e*)	composition of BD[c]
RHF	0.15	99.99	2.00	$0.96sp_{Xe}^{11.78} + 0.28sp_{Au}^{0.07}$
MP2	0.23	99.60	1.96	$0.94sp_{Xe}^{19.26} + 0.34sp_{Au}^{0.05}$
BP86	0.25	99.99	2.00	$0.93sp_{Xe}^{15.94} + 0.36sp_{Au}^{0.05}$

[a] Natural population. [b] Bond orbital. [c] The first term is the hybrid of Xe, and the second is the hybrid of Au; other trivial contributions have been omitted; sp^x denotes a hybrid sp orbital in which $x = |C_p|^2/|C_s|^2$.

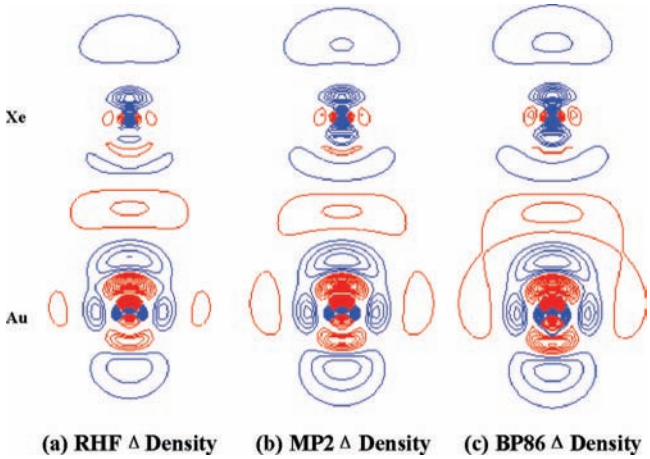

Figure 5. Contour diagrams of the changes in electron density in Au^+Xe for the bonding processes as calculated by the different methods. $\Delta\text{Density} = \text{Density}_{Au^+Xe} - \text{Density}_{Au^+g(Xe)} - \text{Density}_{g(Au)Xe}$. All diagrams were plotted with a maximum contour value of 1000 electrons/a_0^3 and a maximum number of contours of 200000 to amplify the density changes. Red indicates positive sign and blue negative.

the exceptionally strong penetrating effect of the Au 6s orbital, the extra electron density accepted by Au would accumulate around the Au nucleus, and this accounts for the ionic model. However, as mentioned earlier, near the equilibrium internuclear distance, the diffuse Xe 5p orbital reaches the Au center and has a significant overlap with the Au 6s orbital. Consequently, the bonding electrons around the Au center are still shared by the Xe 5p orbital, and this accounts for the covalent model. Thus, the ionic and covalent descriptions for this bond are complementary. They result from the contracted Au 6s and soft Xe 5p orbitals, and our dative polar bond model is still valid.

4. Conclusion

The Au^+Xe system was studied using relativistic model core potentials and a variety of post-Hartree−Fock methods, including MP2, high-level renormalized and completely renormalized coupled-cluster, and density functional theory methods. Potential curves were generated using all of these methods, and D_e, r_e, and vibrational parameters were obtained from the curves. Different correlation spaces were employed in MP2 calculations, and the Xe 4d orbital was found to be nonessential whereas the Au 5p orbital was necessary for the correct results. All of our coupled-cluster results are highly consistent, and use of R- and CR-coupled-cluster methods is unnecessary because of the single-reference nature of the bond-breaking process. Our highest level coupled-cluster results are in excellent agreement with the experimental data for the first Au^+Xe-containing compound. None of our DFT calculations gave credible results. We found that half of the bonding energy stems from the electron correlation. The comparison of potential curves indicates that the Au^+—Xe interaction converges to a charge−induced dipole type of interaction for $R > 4$ Å. The MO diagrams indicate that the weak interaction at the RHF level is due to the incomplete cancelation of contributions between the σ and σ^* orbitals. The NBO analysis points to a polar dative bond between Au^+ and Xe, one that is closer to the covalent limit. A large orbital contribution to the natural bond orbital from the vicinity of Au and Xe nuclei was observed, which can be explained by the relativistic contraction of s- and p-type functions. This feature of the interaction requires that the correct nodal structure of the valence orbitals be represented, and this is the special strength of the model core potential method. The electron density diagrams confirm that the bonding electrons accumulate in the vicinity of Au nucleus. The previous contradictory ionic and covalent models of the bond nature can be reconciled by recognizing the contraction of the Au 6s orbital and the diffuseness of the Xe 5p orbital.

Acknowledgment. The authors are grateful to Dr. M. S. Gordon and Dr. M. W. Schmidt for the original version of the GAMESS program. We appreciate the computing resources of Department of Academic Information and Communication Technologies of University of Alberta that were made available to us. T.Z. expresses his gratitude to Alberta Ingenuity Funds and Killam Trustees for student scholarships. M.K. is grateful to Professor A. J. Sadlej for discussions about relativistic effects. We acknowledge the reviewers for their valuable comments on this work.

References and Notes

(1) Bartlett, N. *Proc. Chem. Soc.* **1962**, 218.
(2) Pyykkö, P. *Chem. Rev.* **1988**, *88*, 563.
(3) Pyykkö, P. *Angew. Chem., Int. Ed.* **2004**, *43*, 4412.
(4) Pyykkö, P. *Inorg. Chim. Acta* **2005**, *358*, 4113.
(5) Pyykkö, P. J. *Am. Chem. Soc.* **1995**, *117*, 2067.
(6) Schröder, D.; Schwarz, H.; Hrusák, J.; Pyykkö, P. *Inorg. Chem.* **1998**, *37*, 624.
(7) Seidel, S.; Seppelt, K. *Science* **2000**, *290*, 117.
(8) Drews, T.; Seidel, S.; Seppelt, K. *Angew. Chem., Int. Ed.* **2002**, *41*, 454.
(9) Hwang, I.-C.; Seidel, S.; Seppelt, K. *Angew. Chem., Int. Ed.* **2003**, *42*, 4392.
(10) Pyykkö, P. *Science* **2000**, *290*, 64.
(11) Read, J. P.; Buckingham, A. D. J. *Am. Chem. Soc.* **1997**, *119*, 9010.
(12) Bellert, D.; Breckenridge, W. H. *Chem. Rev.* **2002**, *102*, 1595.
(13) Hu, W.-P.; Huang, C.-H. *J. Am. Chem. Soc.* **2001**, *123*, 2340.
(14) Berski, S.; Latajka, Z.; Andrés, J. *Chem. Phys. Lett.* **2002**, *356*, 483.
(15) Belpassi, L.; Tarantelli, F.; Sgamellotti, A.; Quiney, H. M.; van Stralen, J. N. P.; Visscher, L. *J. Chem. Phys.* **2007**, *126*, 064314.
(16) Belpassi, L.; Tarantelli, F.; Sgamellotti, A.; Götz, A. W.; Visscher, L. *Chem. Phys. Lett.* **2007**, *442*, 232.
(17) Head-Gordon, M.; Pople, J. A.; Frisch, M. J. *J. Chem. Phys. Lett.* **1988**, *153*, 503.
(18) Frisch, M. J.; Head-Gordon, M.; Pople, J. A. *Chem. Phys. Lett.* **1990**, *166*, 275.
(19) Lee, T. J.; Jayatilaka, D. *Chem. Phys. Lett.* **1993**, *201*, 1.
(20) Head-Gordon, M.; Head-Gordon, T. *Chem. Phys. Lett.* **1994**, *220*, 122.
(21) Saebo, S.; Almlöf, J. *Chem. Phys. Lett.* **1989**, *154*, 83.
(22) Cooke, S. A.; Gerry, M. C. L. *J. Am. Chem. Soc.* **2004**, *123*, 17000.
(23) Ghanty, T. K. *J. Chem. Phys.* **2005**, *123*, 074323.
(24) Lovallo, C. C.; Klobukowski, M. *Chem. Phys. Lett.* **2003**, *368*, 589.
(25) Mane, J. Y.; Klobukowski, M. *Theor. Chem. Acc.* **2004**, *112*, 33.
(26) Nakajima, T.; Hirao, K. *Chem. Phys. Lett.* **1999**, *302*, 383.
(27) Huzinaga, S.; Klobukowski, M. *Chem. Phys. Lett.* **1993**, *212*, 260.

(28) Klobukowski, M. *Chem. Phys. Lett.* **1993**, *214*, 166.
(29) Nakajima, T.; Hirao, K. *Chem. Phys. Lett.* **2000**, *329*, 5111.
(30) Nakajima, T.; Hirao, K. J. *Chem. Phys.* **2000**, *113*, 7786.
(31) Douglas, M.; Kroll, N. M. *Ann. Phys.* **1974**, *82*, 89.
(32) Hess, B. A. *Phys. Rev. A* **1986**, *33*, 3742.
(33) Schwerdtfeger, P.; Brown, J. R.; Laerdahl, J. K. *J. Chem. Phys.* **2000**, *113*, 7110.
(34) Piecuch, P.; Kucharski, S. A.; Kowalski, K.; Musial, M. *Comput. Phys. Commun.* **2002**, *149*, 71.
(35) Piecuch, P.; Kucharski, S. A.; Kowalski, K.; Musial, M. *Comput. Phys. Commun.* **2002**, *149*, 71.
(36) Piecuch, P.; Wloch, M. *J. Chem. Phys.* **2005**, *123*, 224105–1.
(37) Piecuch, P.; Kucharski, S. A.; Kowalski, K.; Musial, M. *J. Chem. Phys.* **2000**, *113*, 18.
(38) Piecuch, P.; Kucharski, S. A.; Kowalski, K.; Musial, M. *J. Chem. Phys.* **2000**, *113*, 5644.
(39) Becke, A. D. *Phys. Rev. A* **1988**, *38*, 3098.
(40) Perdew, J. P. *Phys. Rev. B* **1986**, *33*, 8822.
(41) Pyykkö, P. *Chem. Rev.* **1997**, *97*, 597.
(42) Stephens, J. P.; Delvin, F. J.; Chabalowski, C. F.; Frisch, M. J. *J. Phys. Chem.* **1994**, *98*, 11623.
(43) Becke, A. D. *J. Chem. Phys.* **1992**, *96*, 2155.
(44) Becke, A. D. *J. Chem. Phys.* **1992**, *97*, 9173.
(45) Becke, A. D. *J. Chem. Phys.* **1993**, *98*, 5648.
(46) Lee, C.; Yang, W.; Parr, R. G. *Phys. Rev. B* **1988**, *37*, 785.
(47) Ikura, H.; Tsuneda, T.; Yanai, T.; Hirao, K. *J. Chem. Phys.* **2001**, *115*, 3540.
(48) Kumar, A.; Meath, W. J. *Can. J. Chem.* **1985**, *63*, 1616.
(49) Hohm, U.; Kerl, K. *Mol. Phys.* **1990**, *69*, 803.
(50) Andrae, D.; Haussermann, U.; Dolg, M.; Stoll, H.; Preuss, H. *Theor. Chim. Acta* **1990**, *77*, 123.
(51) Nicklass, A.; Stoll, H. *J. Chem. Phys.* **1995**, *102*, 8942.
(52) Wood, J. H.; Boring, A. M. *Phys. Rev. B* **1978**, *18*, 2701.
(53) Foster, J. P.; Weinhold, F. *J. Am. Chem. Soc.* **1980**, *102*, 7211.
(54) Read, A. E.; Curtiss, L. A.; Weinhold, F. *Chem. Rev.* **1988**, *88*, 899.
(55) Weinhold, F.; Landis, C. R. *Chem. Educ. Res. Pract. Eur.* **2001**, *2*, 91.
(56) Schmidt, M. W.; Baldridge, K. K.; Boatz, J. A.; Elbert, S. T.; Gordon, M. S.; Jensen, J. H.; Koseki, S.; Matsunaga, N.; Nguyen, K. A.; Su, S.; Windus, T. L.; Dupuis, M.; Montgomery, J. J. A. *J. Comput. Chem.* **1993**, *14*, 1347.
(57) Bode, B. M.; Gordon, M. S. *J. Mol. Graphics Mod.* **1998**, *16*, 133.
(58) Boys, S. F.; Bernardi, F. *Mol. Phys.* **1970**, *19*, 553.
(59) Lee, T. J.; Taylor, P. R. *Int. J. Quantum Chem.* **1989**, *56*, 199.
(60) Pyykkö, P. *J. Chem. Soc., Faraday Trans. 2* **1979**, *75*, 1256.
(61) Bartlett, N.; Sladky, F. O. In *Comprehensive Inorganic Chemistry*; Bailar, J. C., Emeleus, H. J., Nyholm, R., Trotman-Dickenson, A. F.,Eds.; Pergamon Press: Oxford, U.K., 1973.
(62) Wesendrup, R.; Schwerdtfeger, P. *Angew. Chem., Int. Ed.* **2000**, *39*, 907.

JP8012656